

Circular polarization of gravitational waves from early-Universe helical turbulence

Tina Kahniashvili ^{1,2,3,4,*}, Axel Brandenburg ^{5,6,2,1,†}, Grigol Gogoberidze,^{2,‡} Sayan Mandal ^{7,2,§}
and Alberto Roper Pol ^{8,2,||}¹McWilliams Center for Cosmology and Department of Physics, Carnegie Mellon University, Pittsburgh, Pennsylvania 15213, USA²Faculty of Natural Sciences and Medicine, Ilia State University, 0194 Tbilisi, Georgia³Abastumani Astrophysical Observatory, Tbilisi, GE-0179, Georgia⁴Department of Physics, Laurentian University, Sudbury, Ontario, Canada P3E 2C⁵Nordita, KTH Royal Institute of Technology and Stockholm University, 10691 Stockholm, Sweden⁶Department of Astronomy, AlbaNova University Center, Stockholm University, 10691 Stockholm, Sweden⁷Physics and Astronomy Department, Stony Brook University, Stony Brook, New York 11794, USA⁸Université de Paris, CNRS, Astrophysique et Cosmologie, Paris, F-75013, France

(Received 17 November 2020; accepted 19 January 2021; published 26 February 2021)

We perform direct numerical simulations to compute the net circular polarization of gravitational waves from helical (chiral) turbulent sources in the early Universe for a variety of initial conditions, including driven (stationary) and decaying turbulence. We investigate the resulting gravitational wave signal assuming different turbulent geneses such as magnetically or kinetically driven cases. Under realistic physical conditions in the early Universe we compute numerically the wave number-dependent polarization degree of the gravitational waves. We find that the spectral polarization degree strongly depends on the initial conditions. The peak of the spectral polarization degree occurs at twice the typical wave number of the source, as expected, and for fully helical decaying turbulence, it reaches its maximum of nearly 100% *only* at the peak. We determine the temporal evolution of the turbulent sources as well as the resulting gravitational waves, showing that the dominant contribution to their spectral energy density happens shortly after the activation of the source. Only through an artificially prolonged decay of the turbulence can further increase of the gravitational wave amplitude be achieved. We estimate the detection prospects for the net polarization, arguing that its detection contains *clean* information (including the generation mechanisms, time, and strength) about the sources of possible parity violations in the early Universe.

DOI: [10.1103/PhysRevResearch.3.013193](https://doi.org/10.1103/PhysRevResearch.3.013193)

I. INTRODUCTION

A remarkable possible source of stochastic gravitational waves (GWs) from the early Universe is turbulence in the primordial plasma induced either from cosmological first-order (electroweak or QCD) phase transitions [1–3], or from the primordial magnetic fields that are coupled to the cosmological plasma [4–7]. The GW signal is potentially detectable by the Laser Interferometer Space Antenna (LISA) in the case of strong enough turbulent motions present at the electroweak scale (assuming that the total energy in the turbulence is up to 1%–10% of the total thermal energy at the moment

of generation) [8–12]. Since GWs propagate *almost* freely from the moment of generation until today,¹ the detection of GWs sourced by primordial turbulence will open a new window to understand physical processes in the very early stages of the evolution of the Universe (at the femtoseconds timescale); see Ref. [16] and references therein. Moreover, several theoretical extensions of the standard model (SM) of particle physics and cosmology (which is insufficient to explain the matter-antimatter asymmetry in the Universe) imply parity symmetry² violation at the electroweak energy scale being possibly manifested through helical (chiral) turbulent motions and/or magnetic fields [19,20]. As expected, such parity-violating turbulent sources will produce circularly polarized GWs [21–27] analogously to the GWs produced via Chern-Simons coupling [28,29]. Furthermore, chiral inflationary GWs might be responsible (through the gravitational

*tinatin@andrew.cmu.edu

†brandenb@nordita.org

‡Grigol_Gogoberidze@iliauni.edu.ge

§sayan.mandal@stonybrook.edu

||roperpol@apc.in2p3.fr

Published by the American Physical Society under the terms of the [Creative Commons Attribution 4.0 International](https://creativecommons.org/licenses/by/4.0/) license. Further distribution of this work must maintain attribution to the author(s) and the published article's title, journal citation, and DOI.

¹We discard the GW damping due to neutrino free streaming [13,14] or from anisotropic stresses [15].²The baryon asymmetry of the Universe can be explained through spontaneous lepton number symmetry breaking at a cosmological phase transition [17,18].

anomaly) for gravitational leptogenesis which, in turn, manifests itself in the neutrino sector by being successful in either the Dirac or Majorana neutrino mass scenario [30]. Moreover, the gravitational anomaly effect and, correspondingly, a successful electroweak baryogenesis scenario appear viable in the case when the GWs are generated through helical magnetic fields [31]. Additionally, the primordial magnetic fields that are responsible for the circularly polarized GWs and, correspondingly, for the baryon asymmetry, can serve as seeds for large-scale magnetic fields in the Universe; see Ref. [32] for a review and references therein. Under this consideration the scheme is as follows: helical magnetic fields act as seeds for large-scale magnetic fields, produce circularly polarized GWs, and enable successful lept- and baryogenesis through the gravitational anomaly. Obviously, if detected, the GW polarization can be a *clean* measure of the deviations from the SM and will provide us with a better understanding of the nature of parity symmetry and its violation. In fact, the consideration of the different forms of “driving” is dictated by different possible sources: for scenarios in which the magnetic field is the primary (dominant) source of turbulence (e.g., inflationary or phase transition-generated magnetic fields) we deal with “magnetically driven” turbulence, while turbulence with primary fluid motions (e.g., sound waves) is “kinetically driven,” and could then result in magnetic field generation through dynamo action. This can lead to a growth of the magnetic energy by orders of magnitude even though the kinetic energy of the turbulence decays [7]. However, this is not considered in the present paper.

Each of these sources might be parity symmetry violating ones. As we show below, the polarization spectra are different for different forms of driving, and thus the measurement of these spectra can lead to an identification of the source and the energy scale at which parity violation happened. Interestingly, our results may help us understand the origin of the cosmic seed magnetic field, i.e., it may help discriminate between astrophysical and cosmological magnetogenesis scenarios. Perhaps most importantly, the investigation of the GW background in combination with its polarization might convincingly establish that observations demand a cosmological magnetic field that cannot be generated by a mechanism operating within the confines of the SM.

The detection of circular polarization of the stochastic GW background is a challenging task [33–35], and the planar interferometers cannot measure net polarization in the case of isotropic backgrounds [36,37]. However, the dipolar anisotropy induced by our proper motion with respect to the cosmic reference frame makes it possible to measure the net circular polarization of the stochastic GW background [38,39], and recently it has been shown that the net polarization of GWs could be detected with a signal-to-noise ratio of order one by LISA if the strength of the signal achieves $h_0^2 \Omega_{\text{GW}} \sim 10^{-11}$ (with Ω_{GW} the fraction between the GW energy density and the critical density today $\mathcal{E}_{\text{cr}} = 3H_0^2/(8\pi G)$, with $H_0 = 100h_0 \text{ km s}^{-1} \text{ Mpc}^{-1}$ the Hubble parameter today and G is the gravitational constant) [40]. These findings make it extremely important to properly compute all characteristics (such as the amplitude, the spectral shape, and the polarization degree) of the GW signal from primordial helical (chiral) sources.

When computing the GW signal from early-Universe turbulent sources, previous studies (with the exception of Ref. [41]) assumed stationary hydrodynamic turbulence and a turbulence duration set by a fraction of the Hubble time at the moment of generation (H_\star^{-1}), making it possible to use the simplified GW equation with a discarded term that describes the expansion of the Universe ($\sim H = a^{-1} da/dt_{\text{ph}}$, where t_{ph} denotes the physical time, and a is the scale factor). Moreover, the magnetic field and primordial plasma coupling, and correspondingly, the turbulence decay have been neglected in those analytic studies, making it impossible to study the GW source dynamics and the temporal dependence of the GW amplitude and spectral characteristics beyond the dilution due to the expansion of the universe. These shortcomings will be avoided by numerically simulating nonstationary turbulence with all terms included, allowing for a full coupling between magnetic fields and plasma motions. We apply hydrodynamic and magnetic forcing terms that have a realistic representation of the time dependent generation of turbulence.

II. NUMERICAL MODELING

Recently we have performed direct numerical simulations of magnetohydrodynamic (MHD) turbulence in the early Universe accounting for the expansion of the Universe using the PENCIL CODE [42], and numerically computed the resulting stochastic GW background and relic magnetic fields [41]. To scale out expansion effects, we use appropriately scaled comoving variables and conformal time. The full set of MHD equations is then similar to the usual MHD equations [4], and the GW equation is written for the scaled strains and the comoving total (magnetic and kinetic) traceless-transverse stress tensor T_{ij}^{TT} . These simulations allowed us to conclude that the proper inclusion of coupling effects results in the extension of the GW spectrum at lower frequencies due to the power transfer at large scales, until the causal horizon determined by the comoving Hubble frequency, $f_H = 1.65 \times 10^{-5} \text{ Hz } (g_\star/100)^{1/6} (T_\star/100 \text{ GeV})$ with g_\star and T_\star being the relativistic degrees of freedom and the temperature at the moment of the GW source activation. In terms of the GW energy density per logarithmic frequency interval as a fraction of critical density today, $h_0^2 \Omega_{\text{GW}}(f)$, the spectrum in the frequency range $f_H \leq f \leq f_S$ (where the typical frequency of the source is $f_S = 2Nf_H^3$, and N determines the number of turbulent eddies per linear Hubble length scale⁴ is $\propto f$, as opposed to f^3 for the causal low-frequency ($f < f_H$) tail obtained analytically [11], while in terms of the *comoving* dimensionless strain amplitude h_c , conventionally written as $h_c(f) = 1.263 \times 10^{-18} (f/1 \text{ Hz})^{-1} [h_0 \Omega_{\text{GW}}(f)]^{1/2}$ [43], we observe the scaling $h_c \propto f^{-1/2}$ in the frequency range $f_H < f < f_S$. At this point we distinguish three parts of $\Omega_{\text{GW}}(f)$: the low-frequency region below the causal horizon $f < f_H$,

³The factor “2” is due to the quadratic nature of the turbulent source.

⁴The parameter N is determined by the physical stirring wave number of the source k_0^{phys} via $H_\star/N = 2\pi/k_0^{\text{phys}}$, and to the comoving peak wave number through $k_0 = k_0^{\text{phys}}(a_\star/a_0)$. Here a_\star and a_0 are scale factors corresponding to the moment of generation and today, and $a_\star/a_0 = 8.0 \times 10^{-16} (100/g_\star)^{1/3} (100 \text{ GeV}/T_\star)$.

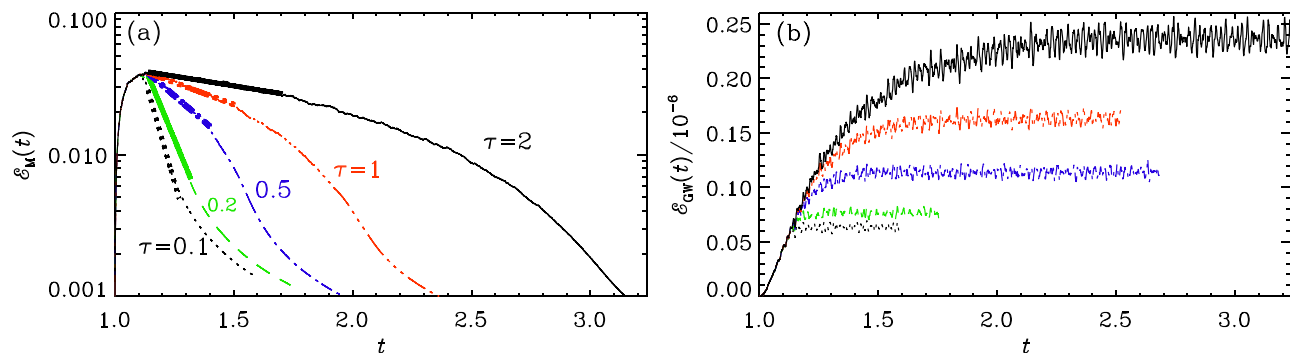


FIG. 1. Evolution of magnetic energy (a) and growth of GW energy density (b) for simulations where the driving is turned off at $t = 1.1$ (black dotted line), or the strength of the driving is reduced linearly in time over the duration $\tau = 0.2$ (green), 0.5 (blue), 1 (red), or 2 (black). Time is in units of the Hubble time at the moment of source activation. The magnetic and GW energy densities are in units of the radiation energy density. In (a), the fat line segments denote a decay proportional to $\exp(\lambda t)$ with λ given in Table I.

the intermediate region $f_H < f < f_S$, and the high-frequency region $f > f_S$. However, due to computational limitations, we are unable to reproduce the entire spectrum in our numerical simulations. At high frequencies, $f > f_S$, numerical simulations agree well with the analytical estimate. In particular, for Kolmogorov turbulence with a slope $-5/3$, the high frequency tail $h_c(f)$ [$\Omega_{\text{GW}}(f)$] scales as $\propto f^{-7/3}$ ($\propto f^{-8/3}$); see Ref. [41] for more details. Earlier work [26] showed that the high-frequency scaling of the GW spectrum depends strongly on the assumptions about the turbulence and the modeling of the time-decorrelation function. Since the spectrum of the stochastic GW background determines the detectability of GWs in a given experiment, realistic turbulence simulations are essential for establishing the sensitivity of upcoming GW experiments to early-Universe physics [43].

III. RESULTS

The spectral form of the GW spectrum at low frequencies is independent of the initial conditions and the turbulence model while the amplitude of the signal strongly depends on the model chosen. The universal form of the GW spectrum does not allow us to discriminate between helical and nonhelical sources and thus limits our ability to determine the parity violation in the early Universe. This leads us to the present study with its main focus on GW circular polarization estimates and the question whether the detection of polarization can help in the identification of distinct properties of the source.

A. Decay with decreased driving

We first address the temporal evolution of the GW spectrum. As it was shown in Ref. [41], the GW spectrum becomes stationary shortly after the driving of the source ends (i.e., when the free decay stage of the source starts), while the energy density of the source is still present. To demonstrate this, we drive magnetic fields with an electromotive force $\mathcal{F}_i = (\delta_{ij} + \sigma \epsilon_{ijl} \hat{k}_l) \mathcal{F}_j^{(0)}$, consisting of plane waves that are delta correlated in time. Here $-1 \leq \sigma \leq 1$ quantifies the fractional helicity, and $\mathcal{F}_j^{(0)}$ is a nonhelical plane-wave forcing term. Plasma motions are self-consistently driven by the Lorentz force. Purely hydrodynamic motions are driven by a ponderomotive force analogous to \mathcal{F}_i .

In Fig. 1 we show the temporal evolution of the source and the growth of the GW energy density for the driven ($1 < t < 1.1$) and decaying stages ($t > 1.1$), where the driving decreases linearly for a duration $\tau = 0.1$ – 2 , although $\tau > 0.5$ may be unrealistic. As in Ref. [41], we use 1152^3 meshpoints for the runs in Fig. 1 and put $\sigma = 0$; see Table I for a summary relevant quantities. During the statistically stationary stage, the GW energy density growth rate is proportional to the duration of turbulence, as was estimated through analytical modeling of Ref. [10]. In reality, the driving stage is short compared to the Hubble timescale, and consists of the few largest eddy turnover times.

In Table I we have quoted the values of $\mathcal{E}_{\text{GW}}^{\text{sat}}$ and $h_{\text{rms}}^{\text{sat}}$ obtained at the end of the simulation at $t = t_{\text{end}}$. We emphasize that \mathcal{E}_{GW} is the comoving GW energy density normalized by the critical energy density, which is the same as the radiation energy density during the simulation, and h_{rms} corresponds to the scaled strain. To compute the relic observable $h_0^2 \Omega_{\text{GW}}$ at the present time, we have to multiply $\mathcal{E}_{\text{GW}}^{\text{sat}}$ by a factor $(H_*/H_0)^2 a_0^{-4}$; see Refs. [41,44] for details, although there we used the symbol Ω_{GW} also for the latter. For the aforementioned fiducial parameters of $g_* = 100$ and $T_* = 100$ GeV, this factor is 1.64×10^{-5} . The largest value of $\mathcal{E}_{\text{GW}}^{\text{sat}}$ quoted in Table I is 2.4×10^{-7} and corresponds therefore to $h_0^2 \Omega_{\text{GW}} = 4 \times 10^{-12}$. Likewise, the values of $h_{\text{rms}}^{\text{sat}}$ in Table I have to be multiplied by $a_0^{-1} = 8.0 \times 10^{-16}$ to obtain the observable h_c at the present time. Again, the largest value of $h_{\text{rms}}^{\text{sat}} = 5.1 \times 10^{-6}$ corresponds therefore to the observable $h_c = 4 \times 10^{-21}$.

B. Approach to a stationary state

The GW generation can be split into three cases (see Fig. 2 for kinetically and magnetically driven turbulence): nonheli-

TABLE I. Characteristic parameters of the runs of Fig. 1.

τ	λ	$\mathcal{E}_M^{\text{max}}$	$\mathcal{E}_K^{\text{max}}$	$\mathcal{E}_{\text{GW}}^{\text{sat}}$	$h_{\text{rms}}^{\text{sat}}$
0.1	-13.5	0.0367	0.0134	6.3×10^{-8}	2.5×10^{-6}
0.2	-9.37	0.0368	0.0135	7.6×10^{-8}	2.8×10^{-6}
0.5	-3.32	0.0372	0.0137	1.1×10^{-7}	3.4×10^{-6}
1	-1.43	0.0378	0.0140	1.6×10^{-7}	4.1×10^{-6}
2	-0.63	0.0381	0.0141	2.4×10^{-7}	5.1×10^{-6}

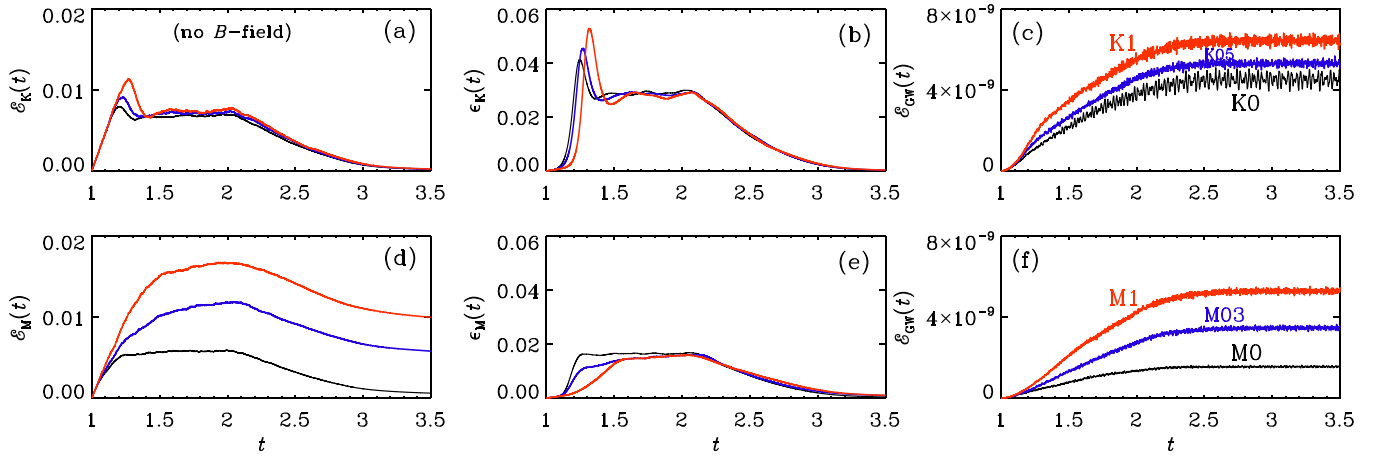


FIG. 2. Evolution of (a) \mathcal{E}_K , (b) ϵ_K , and (c) \mathcal{E}_{GW} for kinetically driven cases with $\sigma = 0$ (run K0, black), 0.5 (run K05, blue), and 1 (run K1, red), and of (d) \mathcal{E}_M , (e) ϵ_M , and (f) \mathcal{E}_{GW} for magnetically driven cases with $\sigma = 0$ (run M0, black), 0.3 (run M03, blue), and 1 (run M1, red).

cal, partially helical ($|\sigma| < 1$), and fully helical. Here we used 512^3 meshpoints and arranged the forcing amplitude such that \mathcal{E}_K and \mathcal{E}_M are around 10^{-2} . The viscosity and magnetic diffusivity have equal values and are chosen such that the dissipative subrange is resolved; see Table II for a summary and Ref. [45] for further details. Surprisingly, the kinetically driven turbulence is more efficient in producing GW energy; see Figs. 2(c) and 2(f). However, in this case the presence of kinetic helicity does not affect the source amplitude—contrary to the magnetically driven case where the amplitude of the source increases substantially with increasing fractional helicity; see Figs. 2(a) and 2(d). We also present the kinetic and magnetic energy dissipation rates, ϵ_K and ϵ_M , respectively. The dissipation rates remain almost unchanged during the stationary stage as we can expect. In addition, we see that they are almost unaffected by the presence of helicity. One may have expected a correlation between ϵ_K (or ϵ_M) and $\mathcal{E}_{\text{GW}}(t)$, but in the magnetically driven case, larger values of σ produce even slightly less dissipation at early times. Nevertheless, $\mathcal{E}_{\text{GW}}(t)$ clearly increases with σ .

C. Polarization degree

To estimate the polarization degree, we follow the procedure described in Ref. [44]. We use the usual circular polar-

ization basis tensors $e_{ij}^\pm = -(\mathbf{e}_1 \pm i\mathbf{e}_2)_i \times (\mathbf{e}_1 \pm i\mathbf{e}_2)_j / \sqrt{2}$, we decompose the Fourier transform of the GW strains $h_{ij}(\mathbf{k}) = \int d^3x e^{i\mathbf{k}\cdot\mathbf{x}} h_{ij}(\mathbf{x})$ into two states—right- (h_+) and left-handed (h_-) circularly polarized GWs $h_{ij} = h_+ e_{ij}^+ + h_- e_{ij}^-$. The GW circular polarization degree is given by [21]⁵

$$\mathcal{P}(k) = \frac{\langle h_+^*(\mathbf{k})h_+(\mathbf{k}') - h_-^*(\mathbf{k})h_-(\mathbf{k}') \rangle}{\langle h_+^*(\mathbf{k})h_+(\mathbf{k}') + h_-^*(\mathbf{k})h_-(\mathbf{k}') \rangle} = \frac{\mathcal{H}(k)}{H(k)}, \quad (1)$$

where $H(k)$ and $\mathcal{H}(k)$ characterize the GW amplitude and polarization (chirality) defined through the Gaussian-distributed GWs wave number-space two-point function (for simplicity of notations we omit the time dependence):

$$\frac{\langle h_{ij}^*(\mathbf{k})h_{lm}(\mathbf{k}') \rangle}{(2\pi)^3} = \delta^{(3)}(\mathbf{k} - \mathbf{k}') [\mathcal{M}_{ijlm}H(k) + i\mathcal{A}_{ijlm}\mathcal{H}(k)],$$

where $4\mathcal{M}_{ijlm}(\hat{\mathbf{k}}) \equiv P_{il}P_{jm} + P_{im}P_{jl} - P_{ij}P_{lm}$, and $8\mathcal{A}_{ijlm}(\hat{\mathbf{k}}) \equiv \hat{\mathbf{k}}_q(P_{jm}\epsilon_{ilq} + P_{il}\epsilon_{jmq} + P_{im}\epsilon_{jlq} + P_{jl}\epsilon_{imq})$ are tensors, $P_{ij}(\hat{\mathbf{k}}) \equiv \delta_{ij} - \hat{k}_i\hat{k}_j$ is the projection operator, and δ_{ij} and ϵ_{ijl} are the Kronecker delta and the fully antisymmetric tensor, respectively.

The GW polarization degree depends, as expected, on the fractional helicity of the source. On the other hand, the evolution of helical sources is determined by the initial fractional helicity: the coupling between the partially helical magnetic field and the plasma motions leads to a reconfiguration of the magnetic field at large scales through free decay, resulting in the growth of the fractional helicity due to the increase of the correlation length and the corresponding decrease of the magnetic energy until the fully helical stage is developed and inverse cascading starts [46]. However, for weakly helical

TABLE II. Characteristic parameters of the runs of Fig. 2.

Run	\mathcal{P}	$\mathcal{E}_M^{\text{max}}$	$\mathcal{E}_K^{\text{max}}$	$\mathcal{E}_{\text{GW}}^{\text{sat}}$	$h_{\text{rms}}^{\text{sat}}$
K0	0.01	0	0.0080	4.5×10^{-9}	7.0×10^{-7}
K01	0.31	0	0.0082	4.4×10^{-9}	6.9×10^{-7}
K03	0.73	0	0.0085	4.8×10^{-9}	6.4×10^{-7}
K05	0.88	0	0.0091	5.3×10^{-9}	5.7×10^{-7}
K1	0.95	0	0.0114	6.4×10^{-9}	5.5×10^{-7}
M0	-0.01	0.0059	0.0020	1.6×10^{-9}	4.1×10^{-7}
M01	0.57	0.0078	0.0021	2.0×10^{-9}	4.6×10^{-7}
M03	0.86	0.0119	0.0024	3.5×10^{-9}	6.9×10^{-7}
M05	0.94	0.0148	0.0026	4.5×10^{-9}	8.6×10^{-7}
M1	0.97	0.0168	0.0025	5.3×10^{-9}	9.0×10^{-7}

⁵As an alternative we can use the decomposition using the linear polarization basis tensors $e_{ij}^+(\hat{\mathbf{k}}) = e_i^+e_j^+ - e_i^-e_j^-$ and $e_{ij}^\times(\hat{\mathbf{k}}) = e_i^+e_j^\times + e_i^\times e_j^+$ as $h_{ij}(\mathbf{k}) = h_+(\mathbf{k})e_{ij}^+(\hat{\mathbf{k}}) + h_\times(\mathbf{k})e_{ij}^\times(\hat{\mathbf{k}})$ where h_+ and h_\times are gauge independent components corresponding to two polarization modes. In this case the polarization degree will be equal to $\mathcal{P}(k) = \langle h_\times^*(\mathbf{k})h_+(\mathbf{k}') - h_+^*(\mathbf{k})h_\times(\mathbf{k}') \rangle / \langle h_+^*(\mathbf{k})h_+(\mathbf{k}') + h_\times^*(\mathbf{k})h_\times(\mathbf{k}') \rangle$.

sources, a substantial time period is needed to reach a fully helical configuration. On the other hand, our simulations show that the dominant contribution to the GW signal occurs shortly after the source has reached its maximum: the subsequent decay of the magnetic field causes a decline of the turbulent driving of GWs. This decline is further enhanced by the expansion of the Universe, although this effect is small if the decay time of the turbulence is short compared with the Hubble time; see Fig. 1. We see that, even with a substantially extended decay phase of the turbulence of twice the Hubble time, the final GW production is enhanced by only a factor of about four. Thus, the GW polarization will retain information about the *initial* fractional helicity of the source.

As we have highlighted above, previous works [21,23] considered stationary turbulence with two different models for helical turbulence realization: (i) Kolmogorov-like helical turbulence with two different spectral slopes, $-5/3$ and $-11/3$ for the spectral energy and helicity densities, $E_M(k)$ and $H_M(k)$, respectively, and (ii) helicity-transferring turbulence (if helicity transfer and small-scale helicity dissipation dominates [47]) with the spectral indices $-7/3$ and $-10/3$ for $E_M(k)$ and $H_M(k)$ [48].⁶ The former case seems most suitable for describing the usual nonhelical turbulence experiencing forward cascading [49]. The difference in using these spectral shapes is determined by the effect of helicity on the energy dissipation length. For highly helical turbulence, the helicity dissipation length is larger, so the two region description [21] might be justified using Kolmogorov-like turbulence at large wave numbers and approximating the low wave number tail with helicity transfer turbulence [50]. Following this description, Ref. [22] and later also Ref. [27] discussed two stages—first the fractionally helical one and later the fully helical one with inverse transfer to describe more precisely the GW generation by helical MHD turbulence. However, these estimates suffer due to (i) the assumption of stationary turbulence; and (ii) neglecting the decay and correspondingly temporal dynamical effects (the GW spectrum becomes stationary shortly after source activation).

D. Dependence on the driving

We now investigate the GW polarization spectra dependence on the nature of driving. We show the polarization degree spectra in Fig. 3 for continuous pumping of kinetic or magnetic energy and helicity at intermediate scales. The parameters of these simulations are the same as those used for Fig. 2; see also Ref. [45]. We see a substantial difference between the kinetic and magnetic initial sources at the low frequency tail due to the inverse cascade for the magnetic sources that is absent in the kinetically driven case: more precisely the energy density spectrum is unchanged after the decay stage starts, while the transfer of magnetic helicity to the large scales results in the increasing of the polarization degree. These results confirm that the polarization degree is

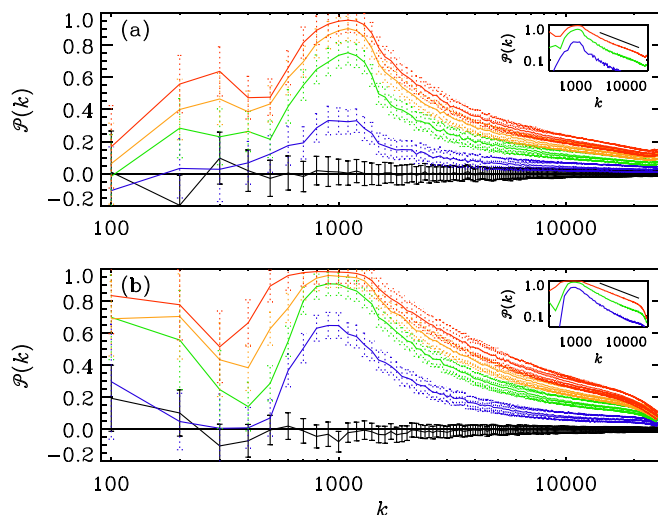


FIG. 3. Degree of circular polarization for (a) kinetically and (b) magnetically forced cases with $\sigma = 0$ (black) 0.1 (blue), 0.3 (green), 0.5 (orange), and 1 (red). Approximate error bars based on the temporal fluctuations and statistical spread for different random seeds of the forcing are shown as solid black lines for $\sigma = 0$ and as dotted lines otherwise. The wave number is in units of the comoving Hubble frequency.

scale dependent: $\propto k^{-0.5}$ at large wave numbers, which is shallower than the k^{-1} expected for Kolmogorov-like helical turbulence with different spectral indices for the magnetic spectral energy density ($n_S = -5/3$) and the spectral helicity density ($n_H = -11/3$). In our simulations, the actual indices are a bit smaller, which also explains the shallower slope in the polarization degree.

E. Comparison of the spectra

In Fig. 4 we show the numerator and denominator of the degree of polarization, $H(k)$ and $\mathcal{H}(k)$, respectively. The underlying kinetic and magnetic energy and helicity spectra are shown in Fig. 5. The figure shows that the GW polarization is larger at larger length scales. To see whether this could be related to inverse cascading in the magnetic case, we now show in Fig. 5 the corresponding energy and helicity spectra. They show clear inverse cascading of the magnetic energy and helicity spectra in the magnetically driven case. Inverse cascading is clearly absent in the kinetic energy and helicity spectra in the kinetically driven case.

The departure from the theoretical predictions is due to the assumption of a scale-independent time-decorrelation function for magnetic energy and helicity densities. Interestingly, the spectral shape of the polarization degree is independent of the actual indices for energy and helicity, but depends on the difference between them [21]. Obviously, in a realistic case, the proper consideration of time decorrelation and its dependence on wave numbers is required. In fact, even in the simplified description, different forms of the time-decorrelation function for different models of turbulence (including both compressible and incompressible cases) and its scale dependence leads to different scaling of the GW spectrum at high frequencies [26].

⁶Note that Ref. [21] used a different convention for the spectral indices referring to the power spectra of the symmetric [$P_S(k) \propto E_M(k)/k^2$] and the antisymmetric parts [$P_A(k) \propto H_M(k)/k$].

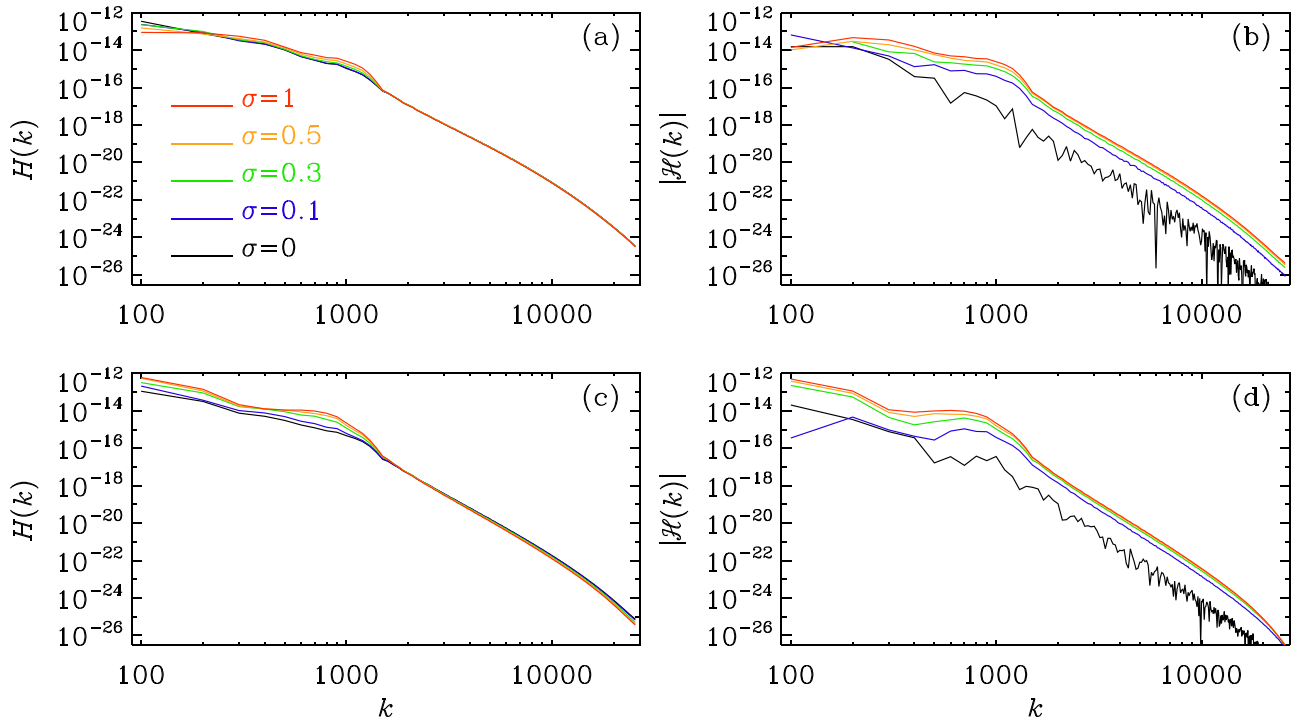


FIG. 4. $H(k)$ (left) and $|\mathcal{H}(k)|$ (right) for (a) and (b) kinetically and (c) and (d) magnetically forced cases with $\sigma = 0$ (runs K0 and M0, black), 0.1 (runs K01 and M01, blue), 0.3 (runs K03 and M03, green), 0.5 (runs K05 and M05, orange), and 1 (runs K1 and M1, red).

IV. CONCLUSIONS

In this paper we present numerical simulations of the circular polarization degree of GWs generated through parity

violating (helical) turbulent sources in the early Universe. We present our results for GWs generated at electroweak energy scales, but the formalism is not limited to the specific

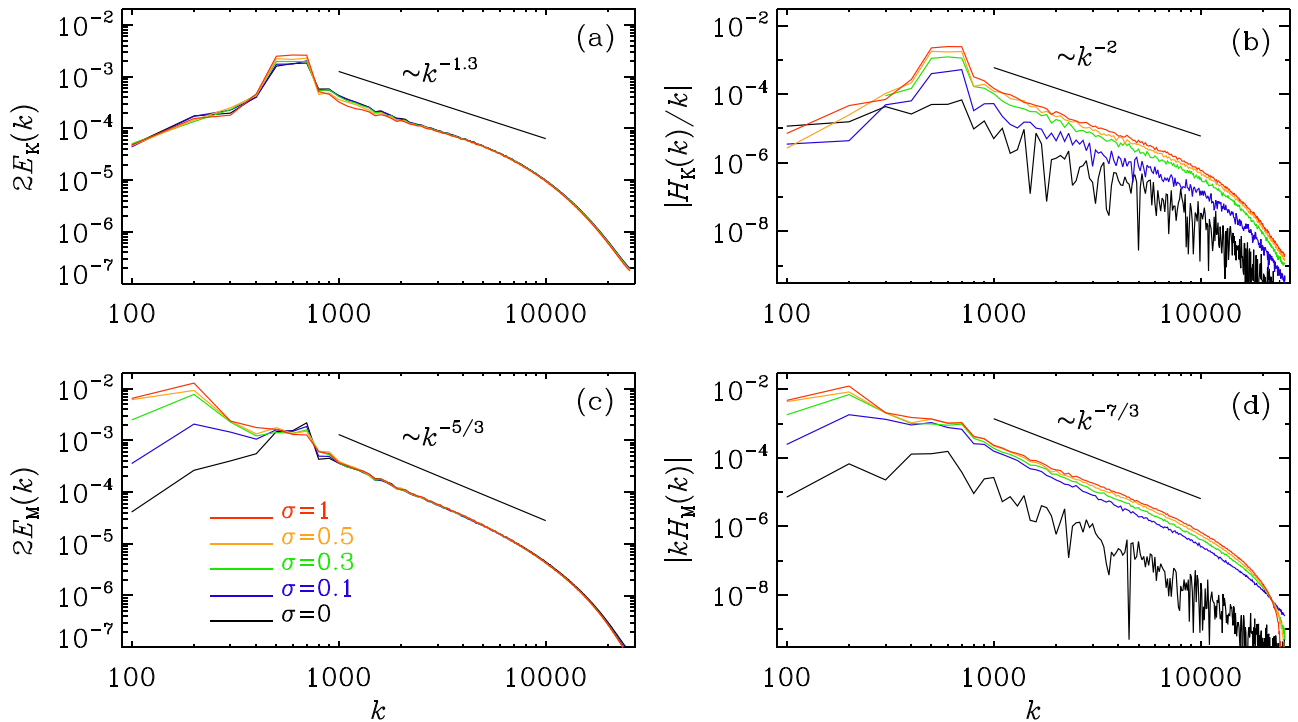


FIG. 5. (a) $2E_K(k)$ and (b) $|H_K(k)/k|$ for kinetically forced cases, and (c) $2E_M(k)$ and (d) $|kH_M(k)|$ for magnetically forced cases with $\sigma = 0$ (runs K0 and M0, black), 0.1 (runs K01 and M01, blue), 0.3 (runs K03 and M03, green), 0.5 (runs K05 and M05, orange), and 1 (runs K1 and M1, red).

moment of GW generation, and can be adjusted to primordial turbulence sources at any time after inflation and before recombination epochs. We have confirmed that the GW signal reaches its maximal strength faster than the turbulence decays. We have also shown that the slope of the low frequency tail of the GW spectrum is independent of the nature of the turbulent source (i.e., the nature of initial driving, the presence of helicity, etc). This restricts the discrimination between helical and nonhelical sources as well between kinetic and magnetic drivings if the signal will be detected. On the other hand, the polarization spectrum not only retains information about the initial characteristic frequency (as well as the GW signal does) and the strength of parity violation of the source, but also manifests the dependence in the driving mechanisms. We have shown that the previously used assumption of stationary turbulence does not predict the GW polarization spectrum for realistic turbulence (the scaling of the spectrum at low and high frequencies, the peak position, etc), and thus might result in inadequate estimates of the detection prospects. In particular, we have shown that the polarization spectra increase at low frequencies due to the inverse cascade, reflecting redistribution of the helical structures, while the energy density of the GWs sustains the scaling that was established soon after the turbulent source activation. In fact, previous works [21,27] predicted a completely different picture for both helical Kolmogorov turbulence and helicity-transferring turbulence. More precisely, no previous work addressed the dependence of the polarization spectra on the temporal characteristics of the source, nor was the helicity transfer-induced increase of polarization spectra at low frequencies detected. There was

never a self-consistent description of GW polarization nor an attempt to disentangle the nature of the underlying source (kinetic vs magnetic driving). Based on our results, we argue that the inverse cascade timescale determines the height of the polarization spectra at low frequencies (a second peak) in the MHD case—even for low fractional helicity. The second (smaller) peak is located at lower frequencies. Fortunately, numerical simulations have now become an affordable tool to address these and other questions of relic GW generation and give a more complete picture for the detection prospects by LISA (as for electroweak phase transitions) and by PTAs (as for QCD phase transitions [51,52]), and/or any future planned missions, including atomic interferometry [53].

The source code used for the simulations of this study, the `PENCIL CODE`, is freely available from Ref. [42]. The simulation setups and the corresponding data are freely available from Ref. [45].

ACKNOWLEDGMENTS

We thank Arthur Kosowsky and Andrii Neronov for useful discussions. Support through the Swedish Research Council, Grant 2019-04234, and Shota Rustaveli GNSF (Grants FR/18-1462 and FR/19-8306) are gratefully acknowledged. We acknowledge the allocation of computing resources provided by the Swedish National Allocations Committee at the Center for Parallel Computers at the Royal Institute of Technology in Stockholm.

-
- [1] M. Kamionkowski, A. Kosowsky, and M. S. Turner, Gravitational radiation from first order phase transitions, *Phys. Rev. D* **49**, 2837 (1994).
 - [2] E. Witten, Cosmic separation of phases, *Phys. Rev. D* **30**, 272 (1984).
 - [3] C. J. Hogan, Gravitational radiation from cosmological phase transitions, *MNRAS* **218**, 629 (1986).
 - [4] A. Brandenburg, K. Enqvist, and P. Olesen, Large scale magnetic fields from hydromagnetic turbulence in the very early universe, *Phys. Rev. D* **54**, 1291 (1996).
 - [5] M. Christensson, M. Hindmarsh, and A. Brandenburg, Inverse cascade in decaying 3-D magnetohydrodynamic turbulence, *Phys. Rev. E* **64**, 056405 (2001).
 - [6] T. Kahniashvili, A. Brandenburg, A. G. Tevzadze, and B. Ratra, Numerical simulations of the decay of primordial magnetic turbulence, *Phys. Rev. D* **81**, 123002 (2010).
 - [7] A. Brandenburg, T. Kahniashvili, S. Mandal, A. Roper Pol, A. G. Tevzadze, and T. Vachaspati, The dynamo effect in decaying helical turbulence, *Phys. Rev. Fluids* **4**, 024608 (2019).
 - [8] A. Kosowsky, A. Mack, and T. Kahniashvili, Gravitational radiation from cosmological turbulence, *Phys. Rev. D* **66**, 024030 (2002).
 - [9] C. Caprini and R. Durrer, Gravitational waves from stochastic relativistic sources: Primordial turbulence and magnetic fields, *Phys. Rev. D* **74**, 063521 (2006).
 - [10] G. Gogoberidze, T. Kahniashvili, and A. Kosowsky, The spectrum of gravitational radiation from primordial turbulence, *Phys. Rev. D* **76**, 083002 (2007).
 - [11] T. Kahniashvili, L. Campanelli, G. Gogoberidze, Y. Maravin, and B. Ratra, Gravitational radiation from primordial helical inverse cascade MHD turbulence, *Phys. Rev. D* **78**, 123006 (2008).
 - [12] C. Caprini, R. Durrer, and G. Servant, The stochastic gravitational wave background from turbulence and magnetic fields generated by a first-order phase transition, *J. Cosmol. Astropart. Phys.* **09** (2009) 024.
 - [13] R. Durrer and T. Kahniashvili, CMB anisotropies caused by gravitational waves: A parameter study, *Helv. Phys. Acta* **71**, 445 (1998).
 - [14] S. Weinberg, Damping of tensor modes in cosmology, *Phys. Rev. D* **69**, 023503 (2004).
 - [15] D. V. Deryagin, D. Y. Grigoriev, V. A. Rubakov, and M. V. Sazhin, Possible anisotropic phases in the early universe and gravitational wave background, *Mod. Phys. Lett. A* **1**, 593 (1986).
 - [16] C. Caprini *et al.*, Detecting gravitational waves from cosmological phase transitions with LISA: An update, *J. Cosmol. Astropart. Phys.* **03** (2020) 024.
 - [17] A. G. Cohen, D. B. Kaplan, and A. E. Nelson, Baryogenesis at the weak phase transition, *Nucl. Phys. B* **349**, 727 (1991).

- [18] A. G. Cohen, D. B. Kaplan, and A. E. Nelson, Weak scale baryogenesis, *Phys. Lett. B* **245**, 561 (1990).
- [19] A. J. Long, E. Sabancilar, and T. Vachaspati, Leptogenesis and primordial magnetic fields, *J. Cosmol. Astropart. Phys.* **02** (2014) 036.
- [20] G. C. Dorsch, S. J. Huber, T. Konstandin, and J. M. No, A second Higgs doublet in the early universe: Baryogenesis and gravitational waves, *J. Cosmol. Astropart. Phys.* **05** (2017) 052.
- [21] T. Kahniashvili, G. Gogoberidze, and B. Ratra, Polarized Cosmological Gravitational Waves from Primordial Helical Turbulence, *Phys. Rev. Lett.* **95**, 151301 (2005).
- [22] T. Kahniashvili, G. Gogoberidze, and B. Ratra, Gravitational Radiation from Primordial Helical MHD Turbulence, *Phys. Rev. Lett.* **100**, 231301 (2008).
- [23] L. Kisslinger and T. Kahniashvili, Polarized gravitational waves from cosmological phase transitions, *Phys. Rev. D* **92**, 043006 (2015).
- [24] S. Alexander, E. McDonough, and D. N. Spergel, Chiral gravitational waves and baryon superfluid dark matter, *J. Cosmol. Astropart. Phys.* **05** (2018) 003.
- [25] S. Anand, J. R. Bhatt, and A. K. Pandey, Chiral plasma instability and primordial gravitational wave, *Eur. Phys. J. C* **79**, 119 (2019).
- [26] P. Niksa, M. Schlegeler, and G. Sigl, Gravitational waves produced by compressible MHD turbulence from cosmological phase transitions, *Class. Quant. Grav.* **35**, 144001 (2018).
- [27] J. Ellis, M. Fairbairn, M. Lewicki, V. Vaskonen, and A. Wickens, Detecting circular polarisation in the stochastic gravitational-wave background from a first-order cosmological phase transition, *J. Cosmol. Astropart. Phys.* **10** (2020) 032.
- [28] S. H. S. Alexander, M. E. Peskin, and M. M. Sheikh-Jabbari, Leptogenesis from Gravity Waves in Models of Inflation, *Phys. Rev. Lett.* **96**, 081301 (2006).
- [29] D. H. Lyth, C. Quimbay, and Y. Rodriguez, Leptogenesis and tensor polarisation from a gravitational Chern-Simons term, *J. High Energy Phys.* **03** (2005) 016.
- [30] P. Adshead, A. J. Long, and E. I. Sfakianakis, Gravitational leptogenesis, reheating, and models of neutrino mass, *Phys. Rev. D* **97**, 043511 (2018).
- [31] H. Abedi, M. Ahmadvand, and S. S. Gousheh, Electroweak baryogenesis via chiral gravitational waves, *Phys. Lett. B* **786**, 35 (2018).
- [32] T. Vachaspati, Progress on cosmological magnetic fields, [arXiv:2010.10525](https://arxiv.org/abs/2010.10525).
- [33] N. Seto, Prospects for Direct Detection of Circular Polarization of Gravitational-Wave Background, *Phys. Rev. Lett.* **97**, 151101 (2006).
- [34] T. L. Smith and R. Caldwell, Sensitivity to a frequency-dependent circular polarization in an isotropic stochastic gravitational wave background, *Phys. Rev. D* **95**, 044036 (2017).
- [35] K. W. Masui, U. L. Pen, and N. Turok, Two- and Three-Dimensional Probes of Parity in Primordial Gravity Waves, *Phys. Rev. Lett.* **118**, 221301 (2017).
- [36] N. Seto and A. Taruya, Measuring a Parity Violation Signature in the Early Universe via Ground-based Laser Interferometers, *Phys. Rev. Lett.* **99**, 121101 (2007).
- [37] N. Seto and A. Taruya, Polarization analysis of gravitational-wave backgrounds from the correlation signals of ground-based interferometers: Measuring a circular-polarization mode, *Phys. Rev. D* **77**, 103001 (2008).
- [38] N. Seto, Quest for circular polarization of gravitational wave background and orbits of laser interferometers in space, *Phys. Rev. D* **75**, 061302(R) (2007).
- [39] S. G. Crowder, R. Namba, V. Mandic, S. Mukohyama, and M. Peloso, Measurement of parity violation in the early universe using gravitational-wave detectors, *Phys. Lett. B* **726**, 66 (2013).
- [40] V. Domcke, J. Garcia-Bellido, M. Peloso, M. Pieroni, A. Ricciardone, L. Sorbo, and G. Tasinato, Measuring the net circular polarization of the stochastic gravitational wave background with interferometers, *J. Cosmol. Astropart. Phys.* **05** (2020) 028.
- [41] A. Roper Pol, S. Mandal, A. Brandenburg, T. Kahniashvili, and A. Kosowsky, Numerical simulations of gravitational waves from early-universe turbulence, *Phys. Rev. D* **102**, 083512 (2020).
- [42] The PENCIL CODE, <https://github.com/pencil-code>, doi: 10.5281/zenodo.2315093
- [43] J. D. Romano and N. J. Cornish, Detection methods for stochastic gravitational-wave backgrounds: A unified treatment, *Living Rev. Rel.* **20**, 2 (2017).
- [44] A. Roper Pol, A. Brandenburg, T. Kahniashvili, A. Kosowsky, and S. Mandal, The timestep constraint in solving the gravitational wave equations sourced by hydromagnetic turbulence, *Geophys. Astrophys. Fluid Dyn.* **114**, 130 (2020)
- [45] T. Kahniashvili, A. Brandenburg, G. Gogoberidze, S. Mandal, and A. Roper Pol, Datasets for “Circular polarization of gravitational waves from early-universe helical turbulence” (v2020.11.07), <https://doi.org/10.5281/zenodo.4256906>; see also <http://www.nordita.org/~brandenb/projects/CircPol/> for easier access.
- [46] A. G. Tevzadze, L. Kisslinger, A. Brandenburg, and T. Kahniashvili, Magnetic fields from QCD phase transitions, *Astrophys. J.* **759**, 54 (2012).
- [47] R. H. Kraichnan, Helical turbulence and absolute equilibrium, *J. Fluid Mech.* **59**, 745 (1973).
- [48] S. S. Moiseev and O. G. Chkhetiani, Helical scaling in turbulence, *Zh. Eksp. Teor. Fiz.* **110**, 357 (1996) [*JETP* **83**, 192 (1996)].
- [49] V. Borue and S. A. Orszag, Spectra in helical three-dimensional homogeneous isotropic turbulence, *Phys. Rev. E* **55**, 7005 (1997).
- [50] P. D. Ditlevsen and P. Giuliani, Cascades in helical turbulence, *Phys. Rev. E* **63**, 036304 (2001).
- [51] C. Caprini, R. Durrer, and X. Siemens, Detection of gravitational waves from the QCD phase transition with pulsar timing arrays, *Phys. Rev. D* **82**, 063511 (2010).
- [52] A. Neronov, A. Roper Pol, C. Caprini, and D. Semikoz, NANOGrav signal from MHD turbulence at QCD phase transition in the early universe, *Phys. Rev. D* **103**, L041302 (2021).
- [53] S. Dimopoulos, P. W. Graham, J. M. Hogan, M. A. Kasevich, and S. Rajendran, Gravitational wave detection with atom interferometry, *Phys. Lett. B* **678**, 37 (2009).